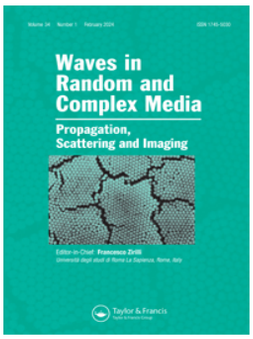

Waves in Random and Complex Media

ISSN: (Print) (Online) Journal homepage: www.tandfonline.com/journals/twrm20

Stability analysis of multi-trigger nano tube sandwich structures considering thermal and magnetic effects

Saman Jolaiy, Armin Yousefi, Zaher Rahimi & Mahdi Bodaghi

To cite this article: Saman Jolaiy, Armin Yousefi, Zaher Rahimi & Mahdi Bodaghi (07 Mar 2024): Stability analysis of multi-trigger nano tube sandwich structures considering thermal and magnetic effects, Waves in Random and Complex Media, DOI: 10.1080/17455030.2024.2326137

To link to this article: https://doi.org/10.1080/17455030.2024.2326137

Published online: 07 Mar 2024.

WAVES IN RANDOM AND COMPLEX MEDIA
https://doi.org/10.1080/17455030.2024.2326137

Taylor & Francis
Taylor & Francis Group

Stability analysis of multi-trigger nano tube sandwich structures considering thermal and magnetic effects

Saman Jolaiy[a], Armin Yousefi[a], Zaher Rahimi[b] and Mahdi Bodaghi[c]

[a]School of Mechanical Engineering, College of Engineering, University of Tehran, Tehran, Iran; [b]School of Engineering and Technology, University of New South Wales, Canberra, Australia; [c]Department of Engineering, School of Science and Technology, Nottingham Trent University, Nottingham, UK

ABSTRACT

This research investigates the stability analysis of multi-trigger nanotube-based sandwich structures that carry fluid subjected to external stimulus. Acrylic-based material and magnetorheological elastomers (MRE) are considered multi-trigger cores in which the external stimulus alters the mechanical properties of the core and, subsequently, the sandwich structures. The system is subjected to an external magnetic field while the ambient temperature varies. The results demonstrate that incorporating a multi-trigger viscoelastic core can accelerate the divergence instability of the non-conservative system while delaying its flutter. Additionally, the impact of the external magnetic field, as a control parameter, for the frequency and stability region of the MRE is more significant than that of the Acrylic-based material. Furthermore, employing Acrylic-based material with a higher shear modulus in a constant magnetic field leads to a more stable system. Moreover, the effect of the external magnetic force on stability is affected smoothly by the ambient temperature. Finally, the influence of temperature on stability is nearly the same for both MRE and Acrylic-based material, with a more pronounced effect observed in systems with larger length-to-diameter ratios.

ARTICLE HISTORY
Received 4 September 2023
Accepted 27 February 2024

KEYWORDS
Multi-trigger sandwich structure; viscoelastic core; stability; magnetic field; temperature source

Nomenclature

u	longitudinal displacement component
u_0	initial longitudinal displacement
v	Lateral displacement component
w	transverse displacements component
x	axial axis
z	transverse axis
ε	strain
σ	normal stress
τ	shear stress
γ	shear strain

CONTACT Zaher Rahimi rahimi.ramyar1@gmail.com

e_0a	nonlocal parameter
E	Young's modulus
G'	storage shear modulus
G''	loss modulus
ρ_f	fluid density
ρ	density
m_t	mass per unit length of tube
m_f	mass per unit length of fluid
ψ_n	the nth shape function
δ	variation operator
I_o	outer layer moment of inertia
I_i	inner layer moment of inertia
δ_{ij}	Kronecker delta
D_o	the outer diameter of the system
Di	the inner diameter of the system
α_{CNT}	*CNT* layers thermal expansion parameter
h	layer thickness
T_0	room temperature
V	volume
A	cross-section area
L	tube length
e_x	unit vector along the X direction
B	magnetic intensity of the longitudinal magnetic field in Tesla
θ	$T - T_0$
T	ambient temperature
K	kinetic energy
W	work done by external forces
π	strain energy
U	fluid velocity
t	time
i	imaginary unit
λ	real part of the eigenvalue
Ω	the imaginary part of the eigenvalue

The subscripts o and i are used for the outer and inner layers.
The subscript f is used to denote the fluid.
The symbol 'CNT' (both as a subscript and superscript) is used to refer to a CNT layer.
The symbol 'C' (both as a subscript and superscript) is used to refer to the core layer.

1. Introduction

Composite sandwich structures are hugely used in the aerospace, automobile, and marine industries because of outstanding properties such as lightweight and high strength-to-weight ratio, corrosion resistance, and excellent energy absorption [1–5]. Sandwich structures with an embedding viscoelastic core with applications of controlling noise and vibration have two elastic parts and a viscoelastic core that effectively dissipates vibration and

acoustic energy [6,7] and has excellent flexural stiffness. Indeed, the viscoelastic layer has a significant role in damping properties [8–10]. Also, these types of structures extended to designing and fabricating structural systems on nano and micro scales due to their ability to provide superior structural and thermal performance [11–15]. Li et al. [16] explored wave propagation in viscoelastic single-walled CNTs while considering the surface effect and exposing it to an in-plane magnetic field. Their findings were based on the nonlocal strain gradient theory. In addition, Karami et al. [17] have analyzed the size-dependent propagation of hygrothermal waves in a viscoelastic graphene sheet in the magnetic field. Their methodology was developed based on the nonlocal strain gradient theory to consider the effects that occur on a small scale. Using Eringen's nonlocal theory, Zenkour and Sobhy [18] could depict the nonlocal vibration of viscoelastic piezoelectric Nano plates with varied boundary conditions while lying on visco-substrate. Pasternak's Radwan and Sobhy [19] have studied the deformation of a viscoelastic graphene sheet with variable boundary conditions immersed in a visco-Pasternak medium and subjected to a time-harmonic thermal load. Their analysis is based on the nonlocal strain gradient theory. Additionally, Sobhy and Zenkour [20] have used the modified couple stress theory to study the bending of viscoelastic nanobeams embedded in a visco-Pasternak medium based on a unique quasi-3D approach. Kolahchi [21] examined wave propagation in a viscoelastic FG-*CNT*s-reinforced plate between two piezoelectric layers.

Viscoelastic materials are among the materials used for sandwich structures, leading to selected mechanical properties [22–26]. Furthermore, incorporating a viscoelastic core into the system results in a modification of the loss factor and dynamic specifications of the construction [27]. Magneto rheological elastomer (MRE) and Acrylic-based materials are potential multi-trigger candidates for sandwich structure core. MRE is a new class of materials known as smart materials. Smart materials are new materials with one or more properties altered in response to external stimuli such as thermal or magnetic fields [28,29]. Magnetorheological elastomer (MRE) is a potential candidate for smart sandwich structures [30,31]. These smart materials include MRE fluids, elastomers, foams, and gels [32]. External magnetic fields and thermal sources [33] could change the mechanical properties of these materials. MRE materials can be reversible and transition fast from a liquid to a nearly solid state in the presence of external magnetic fields [34]. This unique feature regulates the vibrations and stability of various constructions [26–28] or controls the microsystems' motion [35]. In the current research we have used the magnetic field trigger to alter the property

Structure instability is known as one of the main sources of failures of many engineering structures [36–40] and has been considered in many nanosystem applications. This analysis is crucial in understanding the structure's behavior and its design concepts. Engineers consider different materials and conditions to control stability in engineering structures. Several researchers have attempted to determine the main controlling parameters. Mohammadimehr and Mehrabi [41] studied the stability and vibration analysis of sandwich nanotubes conveying fluid resting on an orthotropic elastic medium, where the face sheets were made of temperature-dependent composite material. Free vibration and stability analyses of fluid-conveyed sandwich pipe with porous core and graphene platelet reinforced composite in the top and bottom layers of face sheets were analyzed by Nejadi et al. [42]. Mohajeri et al. [43] studied the dynamic instability, static buckling, and free vibration of the Magnetorheological fluid sandwich plates subjected to a periodic load. They

concluded that increasing the Magnetorheological fluid thickness leads to stabilizing the dynamic instability of sandwich plates.

Moreover, the vibration analysis and energy capability of a sandwich axisymmetric curved panel made of two graphene nanoplatelets reinforced composite face sheets and electro-rheological core was presented for the first time by Shen et al. [26]. MRE and Acrylic-based material materials are also considered in sandwich nanostructures, where the vibration behavior of viscous-elastically coupled sandwich beams and plates was demonstrated by Ghorbanpour Arani et al. [44–46]. They showed that the modal loss factor decreases by increasing magnetic field intensity. In another work by Amiri et al.[47] a parametric stability analysis of a microtube conveying fluid made MRE presented using modified couple stress theory, and more recently, Mihankhah et al. [48] considered free vibration of the sandwich plate made of two smart magnetostrictive face sheets and an electro-rheological fluid core, that considers the behavior of the electro-rheological fluid material under electric field.

Among nanosystems, carbon nanotubes are a group of mechanical elements with enormous applications in different fields, such as cancer treatment methodologies, bioengineering, biosensing, gene therapy, neurology [49–52], wastewater treatment [53,54], microelectronics [55], remediation of emerging pollutants [56] and electromagnetic shielding applications [57]. In almost all its applications, the stability of nanotubes conveying fluid should be considered. Based on the literature review and the authors' best knowledge, the dynamic analysis of multi-trigger nanotube-based sandwich structures conveying fluid with MRE and Acrylic-based material core under an external magnetic field has not been considered so far, specifically when the ambient temperature is changed. In the present study, two different sandwich structures with the investigated MRE and an Acrylic-based material core are considered, and the structures' response to external thermal stimulus and the magnetic field is investigated MRE and an Acrylic-based material core are considered and structures' response to external thermal stimulus and the magnetic field is investigated. Bringing MRE materials makes it possible to analyze the effects of viscoelastic core on the stability of the nanostructure and the amount of energy that can be damped by adding this material to the system, specifically when MRE mechanical properties could be completely changed due to the applied magnetics and ambient temperature. A multi-trigger nanotube-based sandwich structure conveying fluid with a viscoelastic core is proposed. It has potential applications in bioengineering, medicine, wastewater treatment, microelectronics, remediation of emerging pollutants, and electromagnetic shields, as presented in Figure 1. The design's vibration and stability are comprehensively studied. The motion equation is obtained using extended Hamilton's principle using Eringen nonlocal elasticity theory and then solved by extended Galerkin method. Finally, the effects of different parameters, including viscoelastic core thickness, viscoelastic shear modulus (which is a function of magnetic field and ambient temperature), the ratio of diameter to length, magnetic field, and ambient temperature effects are investigated on the flutter and divergence instability of the system.

2. Formulation

This section examines the dynamic motion equation of a multi-trigger three-layer nanotube-based sandwich structure that carries fluid and contains a viscoelastic core made of two different cores: MRE and Acrylic-based material. The system comprises outer and

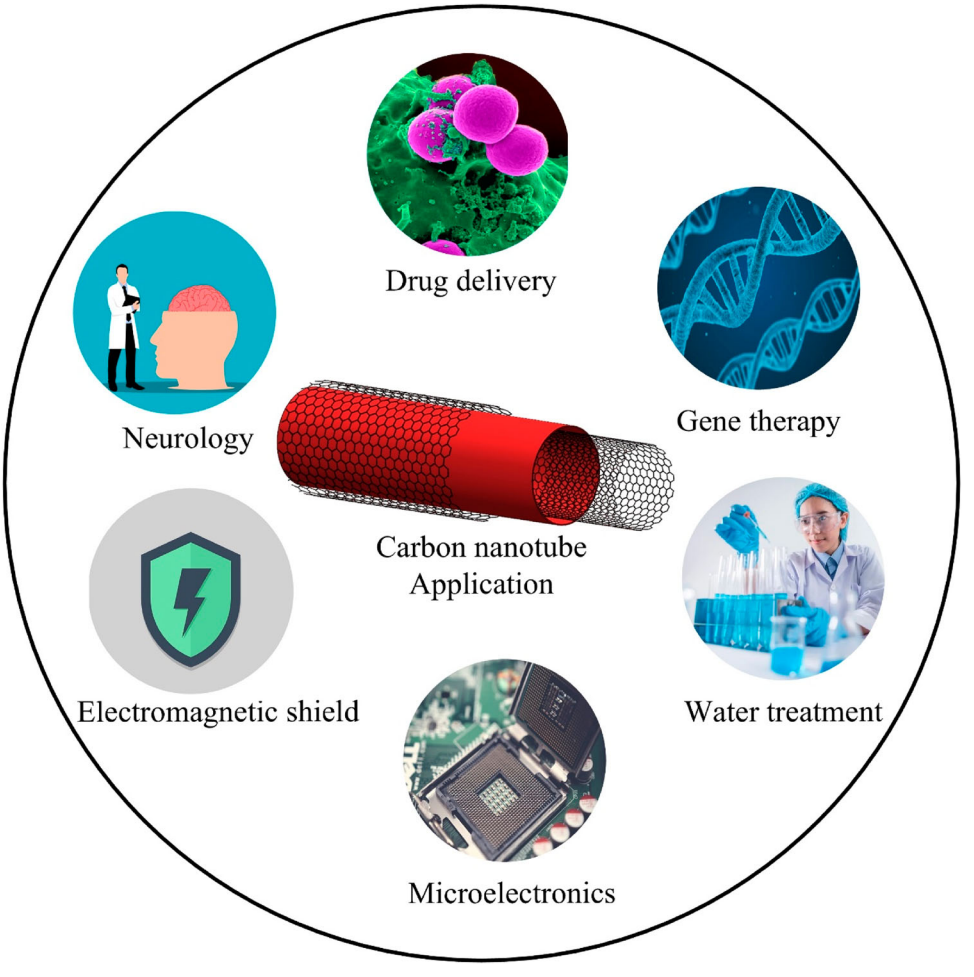

Figure 1. Potential applications of sandwich structures.

inner elastic layers and the viscoelastic core, as illustrated in Figure 2. Following the possible manufacturing processes that can be adopted for the current system have been discussed briefly; however, it must be pointed out that manufacturing the proposed design can be challenging and demands dedicating more time to research and experimental investigation.

The layer-by-layer assembly method is one of the most effective ways to manufacture a three-layer nanotube-based sandwich structure. The original concept of Layer-by-Layer (LbL) assembly was introduced by Iler in 1966, demonstrating the deposition of oppositely charged silica and alumina particles [58].

Also, almost at the same time, Decher and colleagues created thin films through the alternating adsorption of oppositely charged polyelectrolytes [59]. Recently, LbL approaches have garnered significant attention owing to their adaptability in tailoring the size, composition, porosity, stability, and surface functionality of resulting thin films. This is achieved by incorporating multiple functionalities straightforwardly and cost-effectively

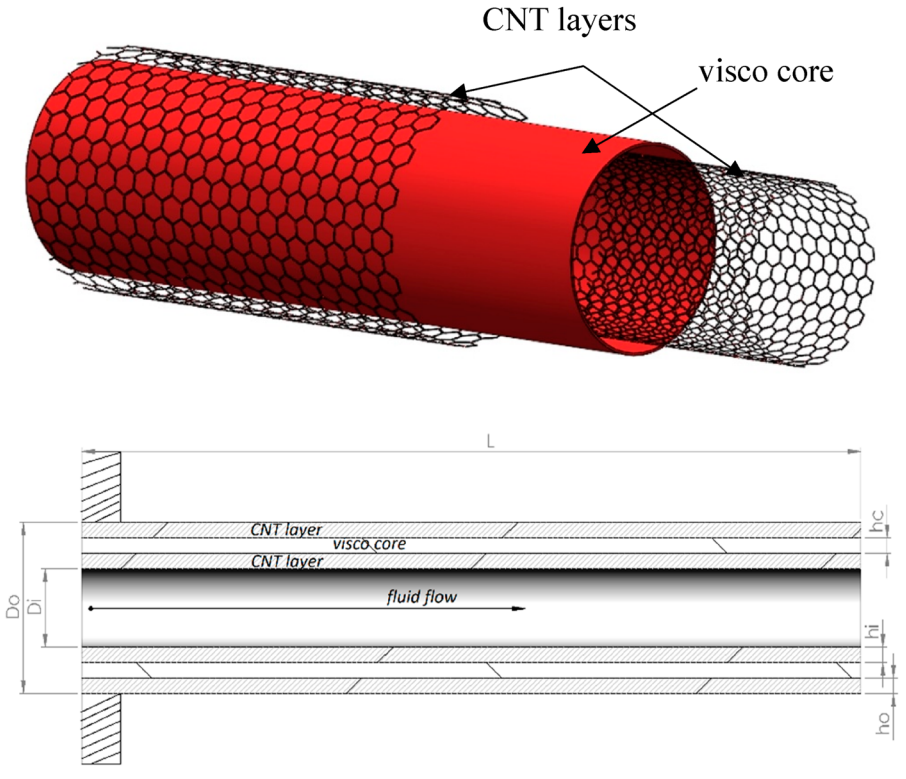

Figure 2. A cantilever nanotube-based sandwich structure with a viscoelastic core conveying fluid.

[59]. Thin films assembled through LbL involve the sequential adsorption of various macromolecular components characterized by attractive forces such as electrostatic interactions, hydrogen bonding, and van der Waals forces [59].

Another viable, cost-effective method to fabricate MEMS devices and tubular hollow microfluidic resonators is the silicon-on-nothing (SON) method [60–62]. Kim et al. [60] explain a simple, cost-effective method employing a SON approach to manufacture tubular hollow microfluidic resonators. The distinctive attributes of this innovative manufacturing method enable the broad application of hollow microtube resonators, their seamless integration across various research domains, and the development of economically feasible devices. Moreover, Kim et al., after the fabrication of tubular hollow microfluidic, proposed an effective way to assess the functionality of the hollow microtube resonators: a device mounting clamp that has been specifically engineered and fabricated. The mounting clamp comprises stainless steel for the top and bottom clamp components, a fluorinated rubber gasket, double O-rings, a quartz window, a piezoelectric actuator, and a piezo fastener [60]. The proposed device can be employed to validate the current model by modifying it.

Using beam theory, the displacements filed are [63]:

$$u(x,z,t) = u_0(x,t) - z\frac{\partial w(x,t)}{\partial x}, \tag{1}$$

$$v(x,z,t) = 0, w(x,z,t) = w(x,t),$$

Considering the neutral axis coincide with the center axial of the tubethen $u_0(x,t) = 0$. Next, only the non-zero strain term and then strain-stress relations for *CNT* layers and viscoelastic are defined. For the outer and the inner elastic layers, the relationships between strains and stresses using nonlocal elasticity theory are [64,65]:

$$\varepsilon_{xx}^{CNT}(x,t) = -z\frac{\partial^2 w(x,t)}{\partial x^2}, \tag{2a}$$

$$\sigma_{xx}^{CNT}(x,t) - (e_0 a)^2 \frac{\partial^2 \sigma_{xx}^{CNT}(x,t)}{\partial x^2} = -zE_{CNT}\frac{\partial^2 w(x,t)}{\partial x^2}, \tag{2b}$$

next, for the viscoelastic core, the shear strain $\gamma^c$is [66–68]:

$$\gamma_{xz}^c = \frac{\partial w^c(x,t)}{\partial x} + \frac{\partial u^c(x,t)}{\partial z}, \tag{3}$$

where

$$\frac{\partial u^c(x,t)}{\partial z} = \left(\frac{h_o + h_i}{2h_c}\right)\frac{\partial w(x,t)}{\partial x} + \left(\frac{u_o - u_i}{h_c}\right), u_o = u_i = 0, \tag{4}$$

then substituting Equation 4 into Equation 3, γ_{xz}^c is:

$$\gamma_{xz}^c = \frac{d}{h_c}\frac{\partial w(x,t)}{\partial x}, d = h_c + \frac{1}{2}(h_o + h_i), \tag{5}$$

the relationship between shear stress and shear strain in the viscoelastic core is [69]:

$$\tau_{xz}^c = G^* \gamma_{xz}^c, \tag{6}$$

$$G^* = G' + iG'', \tag{7}$$

then implementing nonlocal elasticity theory leads to:

$$\tau_{xz}^c(x,t) - (e_0 a)^2 \frac{\partial^2 \tau_{xz}^c(x,t)}{\partial x^2} = \frac{d}{h_c} G^* \frac{\partial^2 w(x,t)}{\partial x^2}. \tag{8}$$

2.1. Magnetic field and ambient temperature effects

The magnetic force along the direction of the flexural displacement effect on the system due to a longitudinal magnetic field $\bar{B} = Be_x$ [70]:

$$F_B(x,t) = \frac{1}{\eta} B^2 A \frac{\partial^2 w(x,t)}{\partial x^2}. \tag{9}$$

Moreover, considering the system in an environment with a variable ambient temperature causes an axial force that affects the tube [71]:

$$F_{thermal} = -(2\alpha_{CNT} E_{CNT} A_{CNT} \theta), \tag{10}$$

where the normal stress term of the viscoelastic core is zero.

2.2. Hamilton principle

To obtain the motion equation, according to extended Hamilton's principle [72,73]:

$$\delta\int_{t_1}^{t_2}\left(\pi - W - K + \frac{1}{2}m_f U^2\int_0^L\left(\frac{\partial^2 w(x,t)}{\partial x^2}\right)^2\right)dt + \int_{t_1}^{t_2} m_f U\left(\frac{\partial w(x,t)}{\partial t} + U\frac{\partial w(x,t)}{\partial x}\right)\delta w dt, \tag{11}$$

the strain energy of the outer and inner layers is [74,75]

$$\pi^{CNT} = \sum_{m=1}^{2}\frac{1}{2}\int\int\int_{V_{CNT}}\sigma_{ij}^{CNT}\varepsilon_{ij}^{CNT}dv, \tag{12}$$

and for the viscoelastic core it is [76,77]:

$$\pi^{c} = \frac{1}{2}\int\int\int_{V_c}\sigma_{ij}\varepsilon_{ij}dv. \tag{13}$$

Then, the total maximum storage energy in the three-layered structure is obtained by summing Eqs.12 and 13. The total kinetic energy of the system, which includes the energy contributions from water, the viscoelastic core, and the outer and inner CNT layers, is calculated as follows: [44,67]:

$$K = \frac{1}{2}\varrho_f\int\int\int_{V_f}\left[\left(\frac{\partial w(x,t)}{\partial t}\right)^2\right]dv + \sum_{m=1}^{2}\left(\frac{1}{2}\varrho_{CNT}\int\int\int_{CNT}\left[\left(\frac{\partial w(x,t)}{\partial t}\right)^2\right]dv\right)_m$$
$$+ \frac{1}{2}\varrho_c\int\int\int_{c}\left[\left(\frac{\partial w(x,t)}{\partial t}\right)^2\right]dv, \tag{14}$$

and the work done by the distributed transverse magnetic load and axial thermal force is:

$$W = \int_0^L\left(F_B(x,t)w(x,t) - \frac{F_{thermal}}{2}\left(\frac{\partial w(x,t)}{\partial t}\right)^2\right)dx, \tag{15}$$

considering both kinetic and potential energy and performing a variation of the output, the motion equation is derived as:

$$((E_{CNT}I)_i + (E_{CNT}I)_o)\frac{\partial^4 w(x,t)}{\partial x^4} + \left(m_f U^2 - \frac{A_c G^* d^2}{h_c^2} - \frac{B_0^2 A}{\eta} + 2\alpha_{CNT}E_{CNT}A_{CNT}\theta\right)\frac{\partial^2 w(x,t)}{\partial x^2}$$
$$+ 2m_f U\frac{\partial^2 w(x,t)}{\partial x\partial\hat{t}} + (m_t + m_f)\frac{\partial^2 w(x,t)}{\partial t^2}$$
$$- (e_0 a)^2\left(2m_f U\frac{\partial^4 w(x,t)}{\partial x^3\partial\hat{t}} + \left(m_f U^2 - \frac{A_c G^* d^2}{h_c^2} - \frac{B_0^2 A}{\eta}\right.\right.$$
$$\left.\left. + 2\alpha_{CNT}E_{CNT}A_{CNT}\theta\right)\frac{\partial^4 w(x,t)}{\partial x^4} + (m_t + m_f)\frac{\partial^4 w(x,t)}{\partial x^2\partial t^2}\right) = 0. \tag{16}$$

Finally, for convenience following dimensionless parameters are used:

$$\begin{aligned}
&\hat{w} = \frac{w}{L}, \hat{x} = \frac{x}{L}, \quad u = \left(\frac{m_f}{(E_{CNT}I)_i + (E_{CNT}I)_o}\right)^{\frac{1}{2}} LU, \\
&\beta = \frac{m_f}{m_t + m_f}, \hat{t} = \frac{t}{L^2}\sqrt{\frac{(E_{CNT}I)_i + (E_{CNT}I)_o}{m_t + m_f}}, \alpha_0 = \frac{\rho A_c G^* d^2 L^2}{h_c^2((E_{CNT}I)_i + (E_{CNT}I)_o)} \\
&\mu = \frac{e_0 a}{L}, \chi = \frac{B_0^2 A L^2}{\eta((E_{CNT}I)_i + (E_{CNT}I)_o)}, \quad \varphi_{CNT} = \frac{\alpha_{CNT} E_{CNT} A_{CNT} L^2}{(E_{CNT}I)_i + (E_{CNT}I)_o}, \quad \hat{\theta} = \frac{\theta}{T_0}
\end{aligned} \tag{17}$$

then the dimensionless equation of motion is:

$$\begin{aligned}
&\frac{\partial^4 \hat{w}(\hat{x},\hat{t})}{\partial \hat{x}^4} + (u^2 - \alpha_0 - \chi + 2\varphi_{CNT}\hat{\theta})\frac{\partial^2 \hat{w}(\hat{x},\hat{t})}{\partial \hat{x}^2} + 2\beta^2 u \frac{\partial^2 \hat{w}(\hat{x}\hat{t})}{\partial \hat{x}\partial \hat{t}} + \frac{\partial^2 \hat{w}(\hat{x},\hat{t})}{\partial \hat{t}^2} \\
&-\mu^2\left(u\frac{\partial^4 \hat{w}(\hat{x},\hat{t})}{\partial \hat{x}^3 \partial \hat{t}} + (u^2 - \alpha_0 - \chi + 2\varphi_{CNT}\hat{\theta})\frac{\partial^4 \hat{w}(\hat{x},\hat{t})}{\partial \hat{x}^4} + \frac{\partial^4 \hat{w}(\hat{x},\hat{t})}{\partial \hat{x}^2 \partial \hat{t}^2}\right) = 0
\end{aligned} \tag{18}$$

3. Numerical solution

In this section, the numerical solution of the obtained dimensionless equation is proposed using Galerkin residual procedure where the transverse deflection is [78]:

$$\begin{aligned}
w(\hat{x},\hat{t}) &= \sum_{n=1}^{m} \psi_n(\hat{x}) q_n(\hat{t}) \\
q_n(\hat{t}) &= X_1 \exp(\omega_0 \hat{t}), \omega_0 = \lambda + i\Omega.
\end{aligned} \tag{19}$$

$\psi_n(\hat{x})$is the suitable shape function that satisfies the boundary conditions for the cantilever beam, ω_0 is the eigenvalue, and X_1 represents its corresponding eigenvector. It should be noted that the real parts of the eigenvalue $(\lambda)$are modal damping, and imaginary parts (Ω) serve as the frequencies. Using both real and imaginary parts, the dimensionless loss factor (which is the ratio of the imaginary part to the real part) is:

$$\eta = \frac{\Omega}{\lambda}. \tag{20}$$

Now, by substituting Equation 20 into Equation 19 and use a suitable shape function that satisfies the boundary condition of the system:

$$\psi_n(\hat{x}) = (\cosh(\kappa_s \hat{x}) - \cos(\kappa_s \hat{x})) - \left(\frac{\sinh(\kappa_s) - \sin(\kappa_s)}{\cosh(\kappa_s) + \cos(\kappa_s)}\right)(\sinh(\kappa_s \hat{x}) - \sin(\kappa_s \hat{x})), \tag{21}$$

where κ_s is obtained from the root of the following equation:

$$\cosh(\kappa_s)\cos(\kappa_s) + 1 = 0, \tag{22}$$

then, applying the extended Galerkin procedure, a set of coupled ordinary differential equations is obtained:

$$[M]\left\{\ddot{q}(\hat{t})\right\} + [C]\{\dot{q}(\hat{t})\} + [K]\{q(\hat{t})\} = 0, \tag{23}$$

where [*M*], [C], and [K] are the mass, damping, and stiffness matrices, respectively, and define as:

$$M_{ij} = \delta_{ij} - \mu^2 \vartheta_{ij}, \tag{24}$$

$$C_{ij} = 2\beta^{\frac{1}{2}} u\xi_{ij} - 2\mu^2 \beta^{\frac{1}{2}} u\nu_{ij}, \tag{25}$$

$$K_{ij} = (1 - \mu^2(u^2 - \alpha_0 - \chi + 2\varphi_{CNT}\hat{\theta}))\zeta_{ij} + (u^2 - \alpha_0 - \chi + 2\varphi_{CNT}\hat{\theta})\varsigma_{ij}, \tag{26}$$

$$\delta_{ij} = \begin{cases} 1 & i = j \\ 0 & i \neq j \end{cases}, \tag{27}$$

$$\vartheta_{ij} = \begin{cases} \Gamma_i\kappa_i(2 + \Gamma_i\kappa_i) & i = j \\ 4\frac{\kappa_i\kappa_j}{\kappa_i^2 - \kappa_j^2}((-1)^{i+j}(\Gamma_j\kappa_i^3 - \Gamma_i\kappa_j^3) - \kappa_i\kappa_j(\Gamma_i\kappa_i - \Gamma_j\kappa_j)) & i \neq j \end{cases},$$

$$\zeta_{ij} = \begin{cases} \kappa_i^2 & i = j \\ 0 & i \neq j \end{cases},$$

$$\xi_{ij} = \begin{cases} 2 & i = j \\ 4\frac{\kappa_j^2}{\kappa_i^4 - \kappa_j^4}(\kappa_i^2 - (-1)^{i+j}\kappa_j^2) & i \neq j \end{cases},$$

$$\varsigma_{ij} = \begin{cases} \Gamma_i\kappa_i(2 - \Gamma_i\kappa_i) & i = j \\ 4\frac{\kappa_j^2(\Gamma_i\kappa_i - \Gamma_j\kappa_j)}{\kappa_i^4 - \kappa_j^4}(\kappa_i^2 + (-1)^{i+j}\kappa_j^2) & i \neq j \end{cases},$$

$$\nu_{ij} = \begin{cases} -2\Gamma_i^2\kappa_i^2 & i = j \\ 4\frac{\kappa_j^3\kappa_i\Gamma_j\kappa_j}{\kappa_i^4 - \kappa_j^4}(\kappa_i^2 + (-1)^{i+j}\kappa_j^2) & i \neq j \end{cases}.$$

To solve Equation 24, it should transfer into a set of first-order differential equation:

$$\{\dot{z}(\hat{t})\} = [\Lambda]\{z(\hat{t})\}, \tag{29}$$

$$[\Lambda] = \begin{bmatrix} [0] & [I] \\ -[M]^{-1}[K] & -[M]^{-1}[C] \end{bmatrix}, \tag{30}$$

where [*I*] is the unit matrix,$z(\hat{t})$ is the state function and $[\Lambda]$ is the state matrix of the system. Solving the above equation by considering the determinant of the standard eigenvalue problem leads to a system characteristic equation. The roots of this equation consist λ and Ω.

4. Results and discussion

4.1. Verification

The mechanical properties of the system are displayed in Table 1. The system consists of inner and outer layers made of CNT, while the core is composed of MRE and an Acrylic-based material. The core is a homogeneous jelly that comprises three fundamental components: silicon rubber, silicon oil, and iron particles, with a mass fraction of 70% for the ferromagnetic particles. [79–81]. Note that the Acrylic-based material is solely affected by the thermal environment and remains unaffected by external magnetic forces[82]. The values of shear

Table 1. Mechanical properties and dimensions of a three-layer nanotube with viscoelastic core.

Layer	Material	Elastic Modulus E(*GPa*)	Density ρ (kg/m^3)
Inner layer	CNT	3400	2300
Core	MRE	–	5740
	Acrylic-based material	–	970
Outer layer	CNT	3400	2300

modulus for both the MRE and Acrylic-based material, in relation to magnetic force and ambient temperature, have been obtained from previous studies. [81,83].

First, a brief overview of the stability conditions of the system based on eigenvalues is provided, which aids in analyzing the output results. A nanotube system conveying fluid is considered stable if all real parts (λ) of the eigenvalues of the matrix [Λ] are negative. Conversely, it is deemed unstable if any of the real parts are positive. As the velocity increases, the system may lose stability due to flutter or divergence. At a specific point known as the critical velocity point, the real part transitions from negative to zero. Flutter occurs at this point (λ_{cr}) when the imaginary part (Ω) is non-zero, causing the system to lose its dynamic stability. When both the real part and the imaginary part become zero simultaneously ($\lambda_{cr} = \Omega_{cr} = 0$), the system loses its static stability due to divergence, resulting in static buckling of the mode. The critical velocity (u_{cr}) and critical frequency (Ω_{cr}) are defined when the system transitions into instability and the sign of lambda changes from negative to positive ($\lambda_{cr}) = 0$).

In order to demonstrate the reliability of the output results, both the real and imaginary parts of the frequency of a single cantilever tube conveying fluid in compared with Ni et al. [84] in Figure 3. In another case, the result for critical frequency (Ωcr) and dimensionless flutter critical velocity (u_{cr})) in terms of β_{cr}) are compared with Gregory et al.[85] shown in Table 2. Furthermore, Table 3 compares the current study and the works of Ramasamy et al. [61] and Yang et al. [62] regarding pipes with viscoelastic cores. It is evident that there is a satisfactory agreement between the obtained results and the published findings.

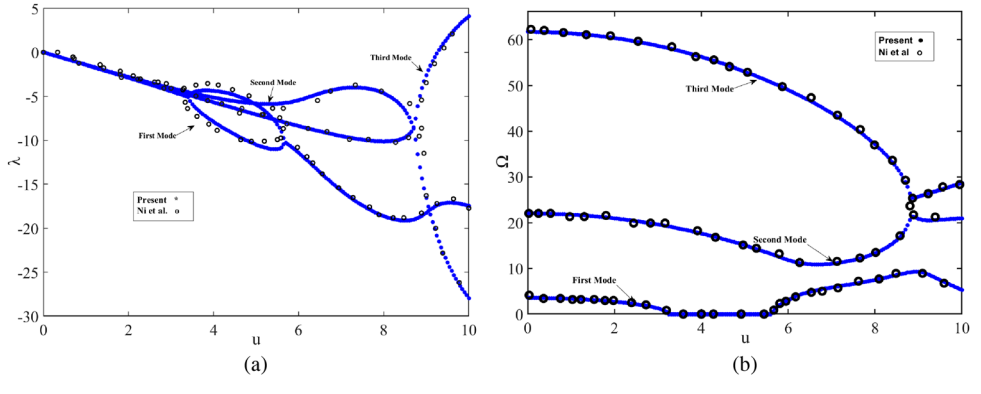

Figure 3. Compares obtained (a) real and (b) imaginary parts of the eigenvalues in the present study with Ni et al. [84].

Table 2. The critical velocity (u_{cr}) and critical frequency (Ω_{cr}) calculated in the present study compared with Gregory et al.[86]. Study.

β_{cr}		0.1	0.2	0.3	0.4	0.5	0.6	0.7	0.8	0.9
u_{cr}	This Study	4.71	5.54	7.06	8.7	9.26	9.92	10.84	13.11	13.95
	Gregory et al	4.7	5.6	7.0	8.5	9.3	9.8	10.5	13.2	14.0
Ω_{cr}	This Study	14.28	14.01	14.97	24.99	26.17	26.39	27.41	40.89	44.05
	Gregory et al[85]	14.4	13.9	1 5	2 5	26.1	26.3	27.6	4 2	4 5

Table 3. Frequency and dimensionless loss factor calculated in the present study compared with Ramasamy et al.[87] and Yang et al.[88].

	Ramasamy et al [87]	Yang et al [88]	present
$f(Hz)$	6.0490	6.0486	6.161
η	0.1455	0.1388	0.1408

4.2. Vibration and stability analysis

The real parts of the first three eigenvalues of the system in Figure 4(a) are shown where the nonlocal parameter is $\mu = 0.01$, the thickness ratio is $h_c/h_o = 1$, and the system is at room temperature in the absence of magnetic force. This diagram clearly illustrates that in the first mode, flutter instability does not occur (based on the explanation of the eigenvalues proposed at the beginning of this section). The first bifurcation (divergence) in the first mode befalls at $u = 3.3$, this point is the critical velocity for the first mode in which the first mode of the system is divided into two branches, and then they meet again at $u = 5.7$. In this domain, the overdamping behavior occurs in the system where the imaginary part is zero (based on Figure 4b). For the second mode, there is no instability. Meanwhile, the stability of the system is different in the third mode where the system is stable for the dimensionless velocity up to about 9 and then loses its stability by fluttering (the real part changes from negative to positive, where the imaginary part is not zero) and this flutter critical velocity for the third mode. Comparing Figure 4 with Figure 3 shows that considering viscoelastic in the core of the nanotube will decrease the starting point of bifrucation of the system for the first mode. At the same time, it increases the critical flutter velocity in the third mode. This comes from the nature of the viscoelastic core, where the static bifrucation causes a reduction of the overall stiffness of the system. Consequently, the softer system loses its stability sooner, while the flutter point adds damping to the system, and this causes an increase of critical flutter velocity for the dynamic system.

To assess the damping effects of the viscoelastic core on the structure's vibration, the first, second and third vibrational mode shapes (that refers to a specific pattern or configuration of movement exhibited by the system when it vibrates at a particular frequency). and dimensionless loss factors are shown in Figure 5. According to the defined dimensionless loss factor and description provided, the structure is stable when the loss factor sign is negative and is unstable when it becomes positive. Based on Figure 5(a), the area that the first mode divaricated and then met again is more visible here, where the loss factor is zero between $u = 3.3$to 5.7. From Figures 5(b) and 4(c), again for the second mode, the system is stable and finally, for the third mode, the critical flutter velocity is around $u_{cr} = 9$ respectively.

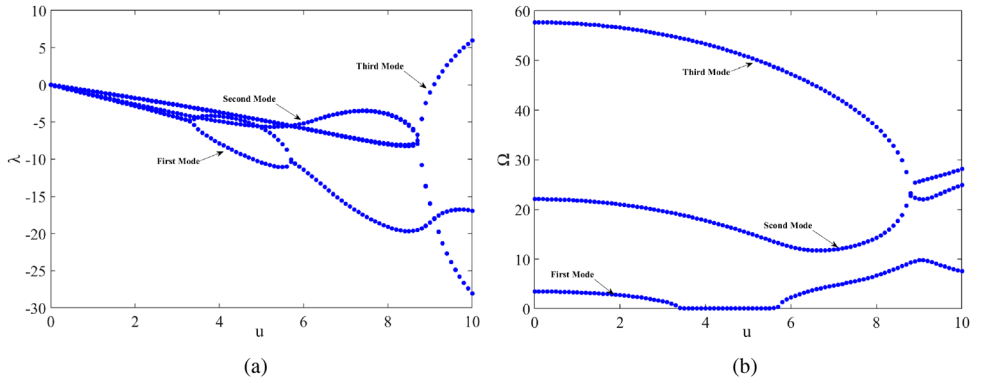

Figure 4. Shows the first three (a) real parts and (b) imaginary parts of eigenvalues when $\beta = 0.5$, $\mu = 0.01$ and $h_c/h_o = 1$.

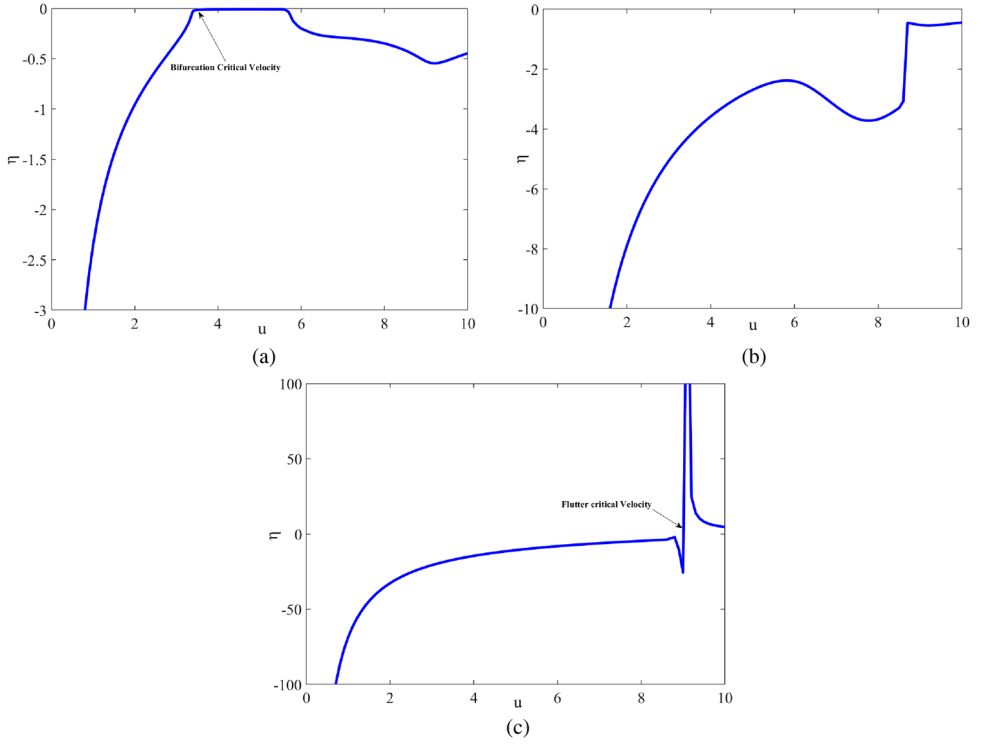

Figure 5. Loss factor for the first three modes when $\beta = 0.5$, $\mu = 0.01$and $h_c/h_o = 1$. (a) first mode, (b) second mode and (c) third mode.

Figure 6 illustrates the natural frequency (Ω) of the system and the real part of the first eigenvalue (λ) in relation to the ratio of the viscoelastic core thickness to the outer layer thickness. It is important to note that the thickness of the outer and inner layers is equal. By increasing the thickness of the core, a bifurcation occurs at a lower velocity, while the rejoining of the bifurcation occurs at a higher velocity. The expansion of the over-damping region is ascribed to an increase in the volume of elastomer arising from a rise in the thickness,

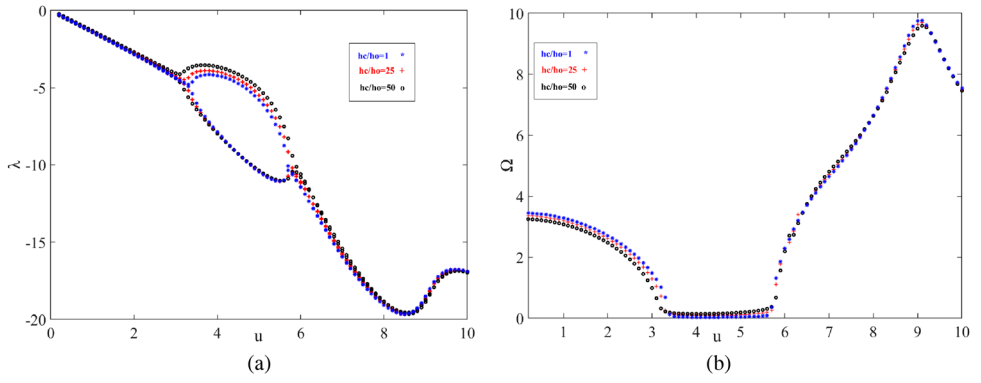

Figure 6. (a) real (λ) and (b) imaginary (Ω) parts of the first eigenvalue in terms of dimensionless velocity for different values of h_c/h_o.

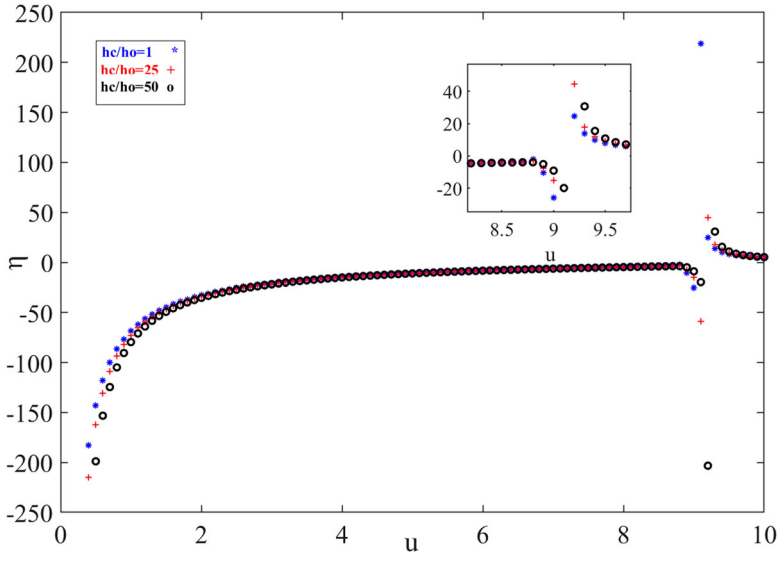

Figure 7. Loss factor of the first mode for different values of h_c/h_o.

which consequently results in a reduction in the stiffness of the system. This observation aligns with Equation 27, where the viscoelastic core's thickness negatively affects the system's overall stiffness. This effect is also evident in the system's natural frequency, as depicted in Figure 6(b), where thicker cores result in a significant reduction in the natural frequency over a wide range of dimensionless velocities.

The effect of the core thickness on flutter instability is illustrated in Figure 7. As the viscoelastic core thickness increases, the point at which the sign changes from negative to positive shifts towards the right side in the third mode. This indicates that flutter occurs at a higher velocity, and stability is maintained at a higher velocity as well.

In Figure 8, the critical frequency (Ω_{cr}) and dimensionless flutter critical velocity (u_{cr}) are depicted in relation to β_{cr} (the ratio of fluid mass to total mass). The diagram is divided into two distinct main areas. The area below the chart represents the stable area, while the

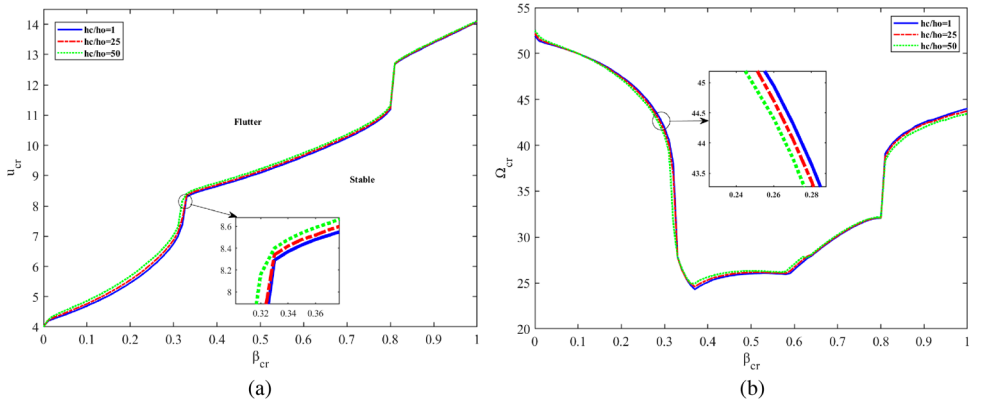

Figure 8. (a) critical frequency and (b) critical flutter velocity in terms of β_{cr} for different h_c/h_o.

area above it corresponds to the flutter area. The boundary lines between these two areas indicate the boundaries of instability.

From Figure 8(b), it can be observed that the system has several S-shaped segments that illustrate a sequence of instability-stabilization-instability that, in comparison with classical tube [84], could be concluded that adding viscoelastic core decreases the sequence of instability-stabilization-instability. In Figure 8, it can be observed that the trends of the boundary line can be broadly classified into three distinct sections. In the first region where β_{cr} is below 0.35, the critical frequency gradually decreases with the increase in the mass ratio β_{cr}. Considering the constancy of the mass of the nanotube in each branch of the graphs, it can be seen that at a low mass ratio, increasing the fluid mass per unit length decreases the critical frequency and increases the critical flutter velocity. The second area is where β_{cr} is between 0.35 and 0.8, both of the graphs climb, but the slope of increase in natural frequency is smother. The thickness ratio enhancement in this area increases the natural frequency and critical flutter velocity. Changes occurring at this point depend on the energy balance between the input energy due to the velocity of the fluid passing through the nanotube, the energy stored by the elastic component, and the energy loss by the viscoelastic core. Finally, the third region is where β_{cr} is greater than 0.8, in this region, increasing the mass ratio and decreasing the thickness ratio increases the natural frequency. After passing $\beta_{cr} = 0.35$, the graphs lines show the S-shaped segments. Finally, someone could conduct that thicker viscoelastic core, increases the critical dimensionless velocity and stability area. This is because the viscoelastic core acts as a damper by absorbing the external energy caused by the fluid's movement and damping the system's instability. The thicker viscoelastic core influences the system stability due to the different nature of the two flutter and divergence phenomena. The thicker core causes more shear deformation, and consequently, the energy is dissipated more intensively; hence it delays flutter instability but supports divergence because of reducing the stiffness of the nanotube structure.

The effect of magnetic force for both MRE and Acrylic-based materials is shown in Figure 9. Forasmuch as the magnetic field does not affect the Acrylic-based material's shear modulus, then for this material, it only effect as external field on the system while for MRE it also changes the shear modulus values. Consequently, the magnetic field effect is

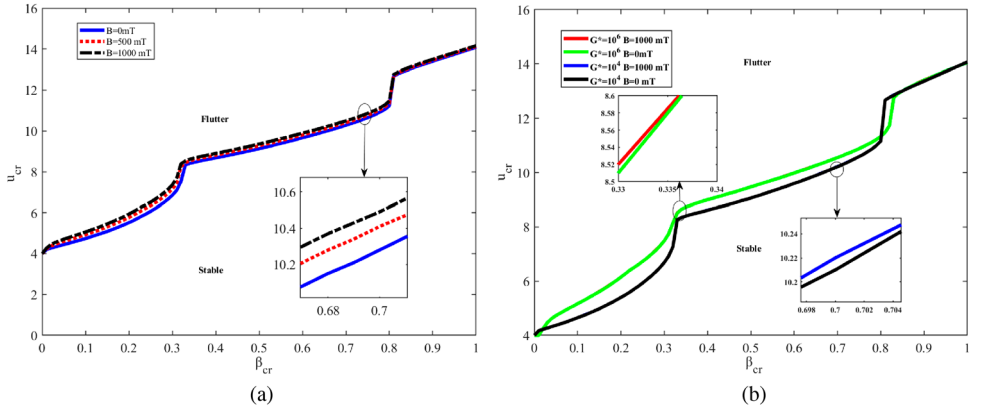

Figure 9. Shows the effect of magnetic field B_0(mT) on critical flutter velocity for (a) MRE and (b) Acrylic-based material.

more pronounced in MRE than in acrylic-based materials. This can be observed by comparing Figures 9(a and b) when increasing the magnetic field strength (B) from 0 to 1000 mT. The trend of this parameter for both materials is the same, where putting the system in a stronger magnetic field increases stability which is visible from inset figures 9(a and b). Overall, the magnetic field causes an increase in the equivalent stiffness of the system. Then it can improve the stability for any kind of material, including Acrylic-based material, while in the case of MRE it also affects the equivalent damping by increasing the shear modulus that enhances the stability. Furthermore, from Figure 9(b), considering Acrylic based-material with a higher shear modulus in a constant magnetic field is more stable.

The effect of ambient temperature on the natural critical frequency and stability region is shown in Figure 10. This graph clearly states that temperature enhancement decreases the critical natural frequency and dimensionless critical velocity. Higher temperature makes the core layer softer by decreasing the shear modulus, And because of the thermal stress term in equation 16, it also affects on outer and inner layers. An increase in temperature has the opposite effect on the loss factor of the MRE core layer, thus causing lower damping effects of the middle layer, and the flutter instability area of the system becomes more expanded, and the tendency of the system to lose stability increases. From Figure 10, also it can be seen that in some points, the diagram of each temperature cross or coincide with each other; this comes from jumping of the experimental shear modulus of MRE material at each temperature (for more details, read Ref. [81])

The effects of the length ratio on the critical frequency and dimensionless flutter critical velocity for MRE are shown in Figure 11. Effects of this ratio in different states are completely different. as can be recognized from Figure 11 for the higher amount of β (more than 0.8) larger L/D_o the ratio drops the critical natural frequency sharply and has no practical effects on flutter critical velocity. While in lower mass ratios, it is entirely contrary. Considering β, a larger L/D_o ratio increases the critical natural frequency and flutter critical velocity gradually. L/D_o Ratio effects can be seen in the centrifugal force of moving fluid. By increasing this ratio, the effects of the velocity decrease, so the centrifugal force of moving fluid decreases, and critical velocity increases. For β_{cr} higher than 0.8, the effect of the fluid Coriolis force

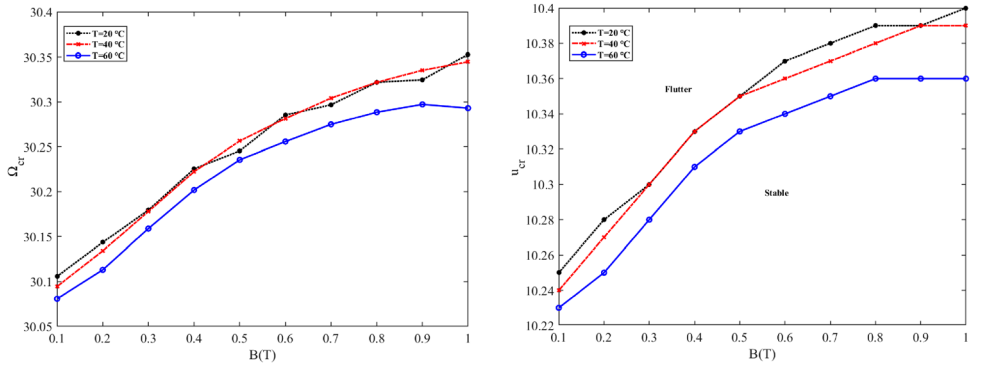

Figure 10. Shows the effect of ambient temperature on (a) critical frequency and (b) critical flutter velocity for MRE.

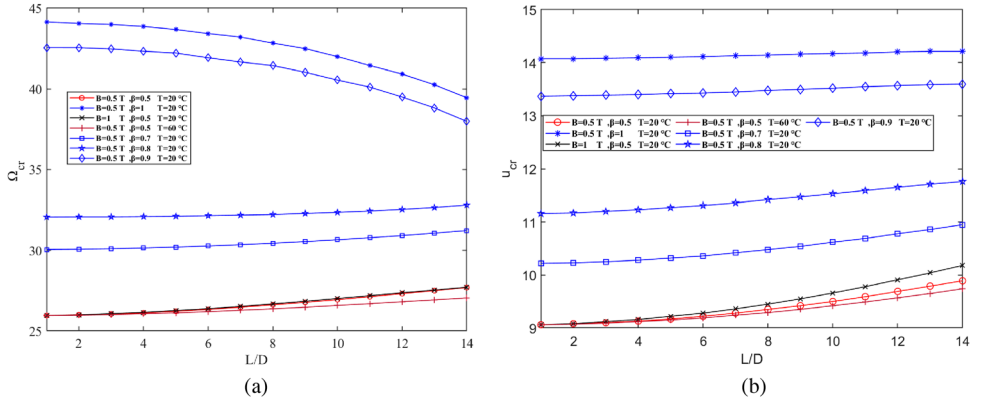

Figure 11. Shows the effects of the length ratio on (a) critical frequency and (b) critical flutter velocity for MRE.

is dominant. This is the turning point between the influencing forces, which is associated with increasing the damping matrix. This is why the trend of the diagram changes. For core layers with a higher shear modulus (Caused by lower temperature or higher magnetic field strength), the slope of the critical speed increase will be higher while it has almost no noticeable effect on the slope of increasing the critical frequency.

In Figure 12, the effect of the ambient temperature on the critical frequency and velocity are shown where $\beta = 0.49, 0.50$and 0.51. The trend of variations is the same with MRE, where an increase in the ambient temperature causes a decrement in both critical frequency and velocity. Although the effect of the temperature between 20–60$^{\circ}C$ on the critical flutter is almost the same, with the range between 30–50 $^{\circ}C$are more effective on decreasing of critical frequency. In Figure 13 can be seen that larger L/D_o ratio leads to a higher critical frequency and velocity while the change is more sensitive in the frequency rather than the flutter velocity, specifically when the ambient temperature is 20 $^{\circ}C$, close to room temperature.

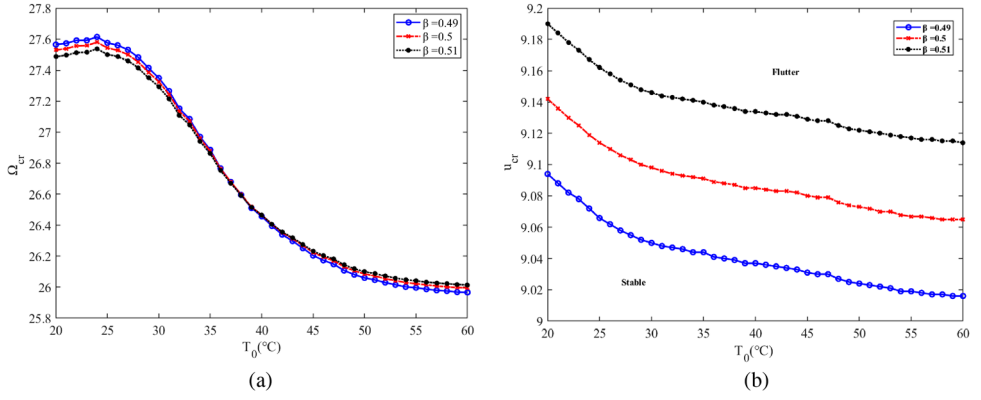

Figure 12. Shows the effect of ambient temperature on (a) critical frequency and (b) critical flutter velocity for Acrylic-based material.

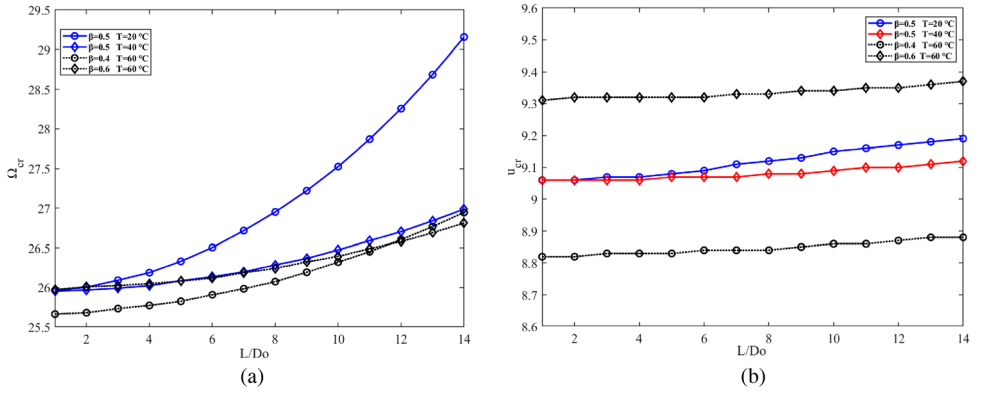

Figure 13. shows the effects of the length ratio on (a) critical frequency and (b) critical flutter velocity for Acrylic-based material.

4.3. Potential applications

Carbon nanotubes have a wide application in medicine. Carbon nanotubes are promising for drug carrier applications in drug delivery. Carbon nanotubes have been employed for drug delivery because of unique features such as significant transporting capabilities, proper surface modifications, and physicochemical features [50]. Several researchers have illustrated the benefit of CNT in brain imaging to recognize a stroke and diseased location, in addition to the delivery of drug molecules to the site of action. Employing CNT for Neurotherapy can be beneficial in treating several neurological pathologies and Neurological disorders, such as ischemic stroke [51,89,90]. In addition, the functionalized CNTs are used for gene delivery by penetrating human cells and delivering the DNA leading to the expression of marker genes [91]. Therefore, the present research, which investigates the stability of three-layer nanotube convening fluid, can provide new insight into future applications in drug delivery.

Another promising application of CNT is wastewater treatment. Carbon nanotubes are used to remove heavy metals, organic and inorganic matter from water. CNTs have some

unique properties, such as large surface area, high aspect ratio, and high chemical and mechanical stabilities, making them perfect candidates to use as adsorbents for water treatment [54]. The stability of CNTs convening fluid, in this case, water, is highly important so that the present research can benefit the water treatment application. Using three-layer sandwich cantilever nanotubes with a viscoelastic core as filler in nanocomposite structures can provide unique thermal and mechanical properties, which leads to new types of structures that can be used for electromagnetic shielding applications [57].

5. Conclusion

The present study focused on the stability analysis of a multi-stimuli (multi-trigger) sandwich structure conveying fluid with a viscoelastic core under an external magnetic field, considering varying ambient temperatures. Two types of smart materials were examined as the viscoelastic core: Acrylic-based material and magnetorheological elastomer (MRE). The shear modulus of the Acrylic-based material was influenced solely by the ambient temperature, while for MRE, it was affected by both the magnetic field and ambient temperature. The main conclusions drawn from the obtained results are as follows:

1- Introducing a smart material as the core of the system leads to quicker divergence instability of the non-conservative system while delaying flutter instability.
2- External magnetic forces can serve as significant control parameters to enhance the stability of the nanotube-based sandwich structures with a viscoelastic core, especially for MRE, owing to the magnetic properties of MRE materials.
3- The effect of the magnetic field is more pronounced for Acrylic-based material with a higher shear modulus.
4- The influence of the external magnetic force on stability exhibits a smooth variation across different ambient temperatures.
5- For MRE, the effect of ambient temperature on stability is less significant compared to the external magnetic force, especially for higher L/D_o ratios.
6- Conversely, for Acrylic-based material, the effect of ambient temperature on stability is more substantial than the external magnetic force, particularly for higher L/D_o ratios.
7- The L/D_o ratio has a greater impact on the critical frequency for Acrylic-based material than MRE, especially when the temperature is near room temperature.
8- Within the 30–50°C range, changing the ambient temperature has the most pronounced effect on the decrement of the critical frequency for Acrylic-based material.

These conclusions highlight the role of viscoelastic materials, magnetic fields, and ambient temperature in the stability analysis of nanotube-based sandwich structures with a smart core conveying fluid, providing insights for potential control and optimization strategies for such systems.

Disclosure statement

No potential conflict of interest was reported by the author(s).

References

[1] Ojha R, Dwivedy S. Parametric instability analysis of sandwich plates with composite skins and LPRE based viscoelastic core. J Sandw Struct Mater. 2020;23(8):3685–3716.

[2] Valvano S, Alaimo A, Orlando C. Analytical analysis of sound transmission in passive damped multilayered shells. Compos Struct. 2020;253:112742. doi: 10.1016/j.compstruct.2020.112742

[3] Safarabadi M, , Haghighi-Yazdi M, Sorkhi MA, Yousefi A, Experimental and numerical study of buckling behavior of foam-filled honeycomb core sandwich panels considering viscoelastic effects. J Sandw Struct Mater. 2020;23(8):3985–4015. doi:10.1177/1099636220975168

[4] Hedayati R, Yousefi A, Bodaghi M. Sandwich structures with repairable cores based on truncated cube cells. Compos Part B: Eng. 2022;243:110124. doi: 10.1016/j.compositesb.2022.110124

[5] Serjouei A, Yousefi A, Jenaki A, et al. 4D printed shape memory sandwich structures: experimental analysis and numerical modeling. Smart Mater Struct. 2022;31(5):055014. doi: 10.1088/1361-665X/ac60b5.

[6] Asadi Jafari MH, Zarastvand M, Zhou J. Doubly curved truss core composite shell system for broadband diffuse acoustic insulation. J Vib Control. 2023: 10775463231206229. doi: 10.1177/10775463231206229

[7] Zarastvand M, Ghassabi M, Talebitooti R. Acoustic insulation characteristics of shell structures: a review. Arch Comput Method E. 2021;28:505–523. doi: 10.1007/s11831-019-09387-z

[8] Lougou KG, Boudaoud Hakim, Daya El Mostafa, Azrar Lahcen, Vibration modeling of large repetitive sandwich structures with viscoelastic core. Mech Adv Mater Struct. 2016;23(4):458–466. doi: 10.1080/15376494.2014.984095

[9] Jolaiy S, et al. Dynamic behaviors of composite leaf springs with viscoelastic cores. Mech Based Des Struct Mach. 2021;51(5):1–23.

[10] Ghafouri M, Ghassabi M, Zarastvand MR, et al. Sound propagation of three-dimensional sandwich panels: influence of three-dimensional Re-entrant auxetic core. AIAA J. 2022;60(11): 6374–6384. doi: 10.2514/1.J061219.

[11] Gao A, et al. Engineering microscale systems for fully autonomous intracellular neural interfaces. Microsy Nanoen. 2020;6(1):1–11. doi: 10.1038/s41378-019-0121-y

[12] Chen H, Opondo NF, Jiang B, et al. Engineering electron–phonon coupling of quantum defects to a semiconfocal acoustic resonator. Nano Lett. 2019;19(10):7021–7027. doi: 10.1021/acs.nanolett.9b02430.

[13] Zhang Z, Wang Y, Zhang H, et al. Hypersonic poration: a New versatile cell poration method to enhance cellular uptake using a piezoelectric nano-electromechanical device. Small. 2017;13(18):1602962), doi: 10.1002/smll.201602962.

[14] Xu W, et al. An all-silicon double differential MEMS accelerometer with improved thermal stability. In 2018 IEEE SENSORS. IEEE; 2018.

[15] Yousefi A, Mashhadi MM, Safarabadi M. Numerical analysis of cracked aluminum plate repaired with multi-scale reinforcement composite patches. J Compos Mater. 2020;54(28):4341–4357. doi: 10.1177/0021998320931177

[16] Li L, Hu Y, Ling L. Wave propagation in viscoelastic single-walled carbon nanotubes with surface effect under magnetic field based on nonlocal strain gradient theory. Physica E. 2016;75:118–124. doi: 10.1016/j.physe.2015.09.028

[17] Karami B, Shahsavari D, Li L. Hygrothermal wave propagation in viscoelastic graphene under in-plane magnetic field based on nonlocal strain gradient theory. Physica E. 2018;97:317–327. doi: 10.1016/j.physe.2017.11.020

[18] Zenkour AM, Sobhy M. Nonlocal piezo-hygrothermal analysis for vibration characteristics of a piezoelectric Kelvin–Voigt viscoelastic nanoplate embedded in a viscoelastic medium. Acta Mech. 2018;229(1):3–19. doi: 10.1007/s00707-017-1920-6

[19] Radwan AF, Sobhy M. A nonlocal strain gradient model for dynamic deformation of orthotropic viscoelastic graphene sheets under time harmonic thermal load. Phys B. 2018;538:74–84. doi: 10.1016/j.physb.2018.03.008

[20] Sobhy M, Zenkour AM. The modified couple stress model for bending of normal deformable viscoelastic nanobeams resting on visco-Pasternak foundations. Mech Adv Mater Struct. 2020;27(7):525–538. doi: 10.1080/15376494.2018.1482579
[21] Kolahchi R, Zarei MS, Hajmohammad MH, et al. Wave propagation of embedded viscoelastic FG-CNT-reinforced sandwich plates integrated with sensor and actuator based on refined zigzag theory. Int J Mech Sci. 2017;130:534–545. doi: 10.1016/j.ijmecsci.2017.06.039.
[22] Keryvin V, Lan M, Bourmaud A, et al. Analysis of flax fibres viscoelastic behaviour at micro and nano scales. Compos Part A: Appl S. 2015;68:219–225. doi: 10.1016/j.compositesa.2014.10.006.
[23] Ilie N, Hickel R. Macro-, micro- and nano-mechanical investigations on silorane and methacrylate-based composites. Dent Mater. 2009;25(6):810–819. doi: 10.1016/j.dental.2009.02.005
[24] Rajabi K, Hosseini-Hashemi S. On the application of viscoelastic orthotropic double-nanoplates systems as nanoscale mass-sensors via the generalized Hooke's law for viscoelastic materials and Eringen's nonlocal elasticity theory. Compos Struct. 2017;180:105–115. doi: 10.1016/j.compstruct.2017.07.085
[25] Altenbach H, Eremeyev VA, Morozov NF. Surface viscoelasticity and effective properties of thin-walled structures at the nanoscale. Int J Eng Sci. 2012;59:83–89. doi: 10.1016/j.ijengsci.2012.03.004
[26] Shen Y, Yin F, Sun P. Vibration analysis and energy capability of sandwich axisymmetric curved panel rested on the novel viscoelastic substrate. Waves Random Complex. 2022: 1–28.
[27] Seilsepour H, Zarastvand M, Talebitooti R. Acoustic insulation characteristics of sandwich composite shell systems with double curvature: the effect of nature of viscoelastic core. J Vib Control. 2023;29(5–6):1076–1090. doi: 10.1177/10775463211056758
[28] Houshangi A, et al. Free damped vibration analysis of a truncated sandwich conical shell with a magnetorheological elastomer core. Waves Random Complex. 2022: 1–28.
[29] Yarali E, Ali Farajzadeh M, Noroozi R, et al. Magnetorheological elastomer composites: modeling and dynamic finite element analysis. Compos Struct. 2020;254:112881. doi: 10.1016/j.compstruct.2020.112881.
[30] Ebrahimi F, Sedighi SB. Wave dispersion characteristics of a rectangular sandwich composite plate with tunable magneto-rheological fluid core rested on a visco-Pasternak foundation. Mech Based Des Struct Mach. 2022;50(1):170–183. doi: 10.1080/15397734.2020.1716244
[31] Rokn-Abadi M, Yousefi M, Haddadpour H, et al. Dynamic stability analysis of a sandwich beam with magnetorheological elastomer core subjected to a follower force. Acta Mech. 2020;231(9):3715–3727. doi: 10.1007/s00707-020-02735-2.
[32] Akhavan H, Ghadiri M, Zajkani A. A new model for the cantilever MEMS actuator in magnetorheological elastomer cored sandwich form considering the fringing field and Casimir effects. Mech Syst Signal Process. 2019;121:551–561. doi: 10.1016/j.ymssp.2018.11.046
[33] Wang D, Zi B, Zeng Y, et al. Temperature-dependent material properties of the components of magnetorheological fluids. J Mater Sci. 2014;49(24):8459–8470. doi: 10.1007/s10853-014-8556-x.
[34] De Vicente J, Klingenberg DJ, Hidalgo-Alvarez R. Magnetorheological fluids: a review. Soft Matter. 2011;7(8):3701–3710. doi: 10.1039/c0sm01221a
[35] Kaluvan S, Thirumavalavan V, Kim S, et al. A new magneto-rheological fluid actuator with application to active motion control. Sens Actuators, A. 2016;239:166–173. doi: 10.1016/j.sna.2016.01.030.
[36] Cedolin L. Stability of structures: elastic, inelastic, fracture and damage theories. Oxford: Oxford University Press; 2010.
[37] Rahimi Z. Vibration analysis of curved nanotube conveying fluid and nanoparticle considering surface and non-local effects. Waves Random Complex. 2021: 1–20.
[38] Xu W, et al. Nonlocal vibration analysis of spinning nanotubes conveying fluid in complex environments. Waves Random Complex. 2021: 1–33.
[39] Wang Y, Jiang X, Babaei H. Nonlinear thermal instability and vibration analysis of pre/post-buckled FG porous nanotubes using nonlocal strain gradient theory. Waves Random Complex. 2021: 1–34.

[40] Mahinzare M, Mohammadi K, Ghadiri M. A nonlocal strain gradient theory for vibration and flutter instability analysis in rotary SWCNT with conveying viscous fluid. Waves Random Complex. 2021;31(2):305–330. doi: 10.1080/17455030.2019.1584420
[41] Mohammadimehr M, Mehrabi M. Stability and free vibration analyses of double-bonded micro composite sandwich cylindrical shells conveying fluid flow. Appl Math Model. 2017;47:685–709. doi: 10.1016/j.apm.2017.03.054
[42] Nejadi M, Mohammadimehr M, Mehrabi M. Free vibration and stability analysis of sandwich pipe by considering porosity and graphene platelet effects on conveying fluid flow. Alexandria Eng J. 2021;60(1):1945–1954. doi: 10.1016/j.aej.2020.11.042
[43] Mohajeri S, et al. Dynamic instability, free vibration, and buckling analysis of MR fluid sandwich plates with FG face layers using the HSDT-based finite strip method. Mech Based Des Struct Mach. 2021;60(1):1–28.
[44] Ghorbanpour Arani A, BabaAkbar Zarei H, Eskandari M, et al. Vibration behavior of viscoelastically coupled sandwich beams with magnetorheological core and three-phase carbon nanotubes/fiber/polymer composite facesheets subjected to external magnetic field. J Sandw Struct Mater. 2019;21(7):2194–2218. doi: 10.1177/1099636217743177.
[45] Ghorbanpour Arani A, BabaAkbar Zarei H, Haghparast E. Vibration response of viscoelastic sandwich plate with magnetorheological fluid core and functionally graded-piezoelectric nanocomposite face sheets. J Vib Control. 2018;24(21):5169–5185.
[46] Kajiwara I, Kitabatake S, Hosoya N, et al. Design of dielectric elastomer actuators for vibration control at high frequencies. Int J Mech Sci. 2019;157:849–857. doi:10.1016/j.ijmecsci.2019.05.019.
[47] Amiri A, Talebitooti R. Prospects of measuring $$R_b$$ in hadronic $${Z}$$ decays at the CEPC. The Eur Phy J Plus. 2021;136(11):1–28. doi: 10.1140/epjp/s13360-020-01001-7
[48] Mihankhah A, et al. Magneto-Rheological response in vibration of intelligent sandwich plate with velocity feedback control. J Solid Mech. 2022;14(4):430–446.
[49] Firme III, P C, Bandaru PR. Toxicity issues in the application of carbon nanotubes to biological systems. Nanomed Nanotechnol Biol Med. 2010;6(2):245–256. doi: 10.1016/j.nano.2009.07.003
[50] Zhang W, Zhang Z, Zhang Y. The application of carbon nanotubes in target drug delivery systems for cancer therapies. Nanoscale Res Lett. 2011;6(1):555. doi: 10.1186/1556-276X-6-555
[51] Nunes A, Al-Jamal K, Nakajima T, et al. Application of carbon nanotubes in neurology: clinical perspectives and toxicological risks. Arch Toxicol. 2012;86(7):1009–1020. doi: 10.1007/s00204-012-0860-0.
[52] Raphey VR, Henna TK, Nivitha KP, et al. Advanced biomedical applications of carbon nanotube. Mater Sci Eng C. 2019;100:616–630. doi: 10.1016/j.msec.2019.03.043.
[53] Yin Z, Cui C, Chen H, et al. The application of carbon nanotube/graphene-based nanomaterials in wastewater treatment. Small. 2020;16(15):1902301. doi: 10.1002/smll.201902301.
[54] Barrejón M, Prato M. Carbon nanotube membranes in water treatment applications. Adv Mater Interfaces. 2022;9(1):2101260. doi: 10.1002/admi.202101260
[55] Hoenlein W, Kreupl F, Duesberg GS, et al. Carbon nanotube applications in microelectronics. IEEE Trans Compon Packag Technol. 2004;27(4):629–634. doi: 10.1109/TCAPT.2004.838876.
[56] Chung JH, Hasyimah N, Hussein N. Application of carbon nanotubes (CNTs) for remediation of emerging pollutants - A review. Trop Aquat Soil Poll. 2021;2(1):13–26. doi: 10.53623/tasp.v2i1.27
[57] Xie Z, Cai Y, Zhan Y, et al. Thermal insulating rubber foams embedded with segregated carbon nanotube networks for electromagnetic shielding applications. Chem Eng J. 2022;435:135118. doi: 10.1016/j.cej.2022.135118.
[58] Iler R. Multilayers of colloidal particles. J Colloid Interface Sci. 1966;21(6):569–594. doi: 10.1016/0095-8522(66)90018-3
[59] Decher G. Fuzzy nanoassemblies: toward layered polymeric multicomposites. Science. 1997;277(5330):1232–1237. doi: 10.1126/science.277.5330.1232
[60] Kim J, Song J, Kim K, et al. Hollow microtube resonators via silicon self-assembly toward subattogram mass sensing applications. Nano Lett. 2016;16(3):1537–1545. doi: 10.1021/acs.nanolett.5b03703.

[61] Jurczak M, Skotnicki T, Paoli M, et al. Silicon-on-Nothing (SON)-an innovative process for advanced CMOS. IEEE Trans Electron Devices. 2000;47(11):2179–2187. doi: 10.1109/16.877181.
[62] Mizushima I, Sato T, Taniguchi S, et al. Empty-space-in-silicon technique for fabricating a silicon-on-nothing structure. Appl Phys Lett. 2000;77(20):3290–3292. doi: 10.1063/1.1324987.
[63] Aguib S, Nour A, Benkoussas B, et al. Numerical simulation of the nonlinear static behavior of composite sandwich beams with a magnetorheological elastomer core. Compos Struct. 2016;139:111–119. doi: 10.1016/j.compstruct.2015.11.075.
[64] Li P, Fang Y, Hu R. Thermoelastic damping in rectangular and circular microplate resonators. J Sound Vib. 2012;331(3):721–733. doi: 10.1016/j.jsv.2011.10.005
[65] Nayfeh AH, Pai PF. Linear and nonlinear structural mechanics. Weinheim: John Wiley & Sons; 2008.
[66] Rajamohan V, Sedaghati R, Rakheja S. Vibration analysis of a multi-layer beam containing magnetorheological fluid. Smart Mater Struct. 2009;19(1):015013. doi:10.1088/0964-1726/19/1/015013
[67] Arvin H, Sadighi M, Ohadi A. A numerical study of free and forced vibration of composite sandwich beam with viscoelastic core. Compos Struct. 2010;92(4):996–1008. doi: 10.1016/j.compstruct.2009.09.047
[68] Mead D, Markus S. The forced vibration of a three-layer, damped sandwich beam with arbitrary boundary conditions. J Sound Vib. 1969;10(2):163–175. doi: 10.1016/0022-460X(69)90193-X
[69] Brinson HF, Brinson LC. Polymer engineering science and viscoelasticity. In An Introduction. 2008.
[70] Sadeghi-Goughari M, Jeon S, Kwon H-J. Effects of magnetic-fluid flow on structural instability of a carbon nanotube conveying nanoflow under a longitudinal magnetic field. Phys Lett A. 2017;381(35):2898–2905. doi: 10.1016/j.physleta.2017.06.054
[71] Benzair A, Tounsi A, Besseghier A, et al. The thermal effect on vibration of single-walled carbon nanotubes using nonlocal Timoshenko beam theory. J Phys D: Appl Phys. 2008;41(22):225404. doi: 10.1088/0022-3727/41/22/225404.
[72] Jin G, Yang C, Liu Z. Polymer-matrix composites carbon fibre characterisation and damage inspection using selectively heating thermography (SeHT) through electromagnetic induction. Compos Struct. 2016;140:590–601. doi: 10.1016/j.compstruct.2016.01.006
[73] Paidoussis MP. *Fluid-structure interactions: slender structures and axial flow*. Vol. 1. Oxford: Academic Press; 1998.
[74] Bishop JE, Kinra VK. Elastothermodynamic damping in laminated composites. Int J Solids Struct. 1997;34(9):1075–1092. doi: 10.1016/S0020-7683(96)00085-6
[75] Parkus H. Thermoelasticity. Wien: Springer Science & Business Media; 2012.
[76] Roylance D. Engineering viscoelasticity. Cambridge (MA): Department of Materials Science and Engineering–Massachusetts Institute of Technology; 2001; 2139: p. 1–37.
[77] Gutierrez-Lemini D. Engineering viscoelasticity. Waltham: Springer; 2014.
[78] Zuo W, Li P, Du J, et al. Thermoelastic damping in trilayered microplate resonators. Int J Mech Sci. 2019;151:595–608. doi: 10.1016/j.ijmecsci.2018.12.015.
[79] Fotsing E, Sola M, Ross A, et al. Dynamic characterization of viscoelastic materials used in composite structures. J Compos Mater. 2014;48(30):3815–3825. doi: 10.1177/0021998313514254.
[80] Feldstein MM, Siegel RA. Molecular and nanoscale factors governing pressure-sensitive adhesion strength of viscoelastic polymers. J Polym Sci, Part B: Polym Phys. 2012;50(11):739–772. doi: 10.1002/polb.23065
[81] Xiang C, Gao P, Liu H, et al. Experimental and theoretical study of temperature-dependent variable stiffness of magnetorheological elastomers. Int J Mater Res. 2018;109(2):113–128. doi: 10.3139/146.111590.
[82] Malaki M, Hashemzadeh Y, Karevan M. Effect of nano-silica on the mechanical properties of acrylic polyurethane coatings. Prog Org Coat. 2016;101:477–485. doi: 10.1016/j.porgcoat.2016.09.012
[83] Wright P. Composition and properties of soft lining materials for acrylic dentures. J Dent. 1981;9(3):210–223. doi: 10.1016/0300-5712(81)90057-9

[84] Ni Q, Zhang Z, Wang L. Application of the differential transformation method to vibration analysis of pipes conveying fluid. Appl Math Comput. 2011;217(16):7028–7038. doi: 10.1016/j.amc.2011.01.116

[85] Gregory R, Paidoussis M. Unstable oscillation of tubular cantilevers conveying fluid I. Theory. Proc R Soc London A Math Phy Sci. 1966;293(1435):512–527.

[86] Gregory R, Paidoussis M. Unstable oscillation of tubular cantilevers conveying fluid II. *Experiments*. Proc R Soc London A Math Phy Sci. 1966;293(1435):528–542.

[87] Ramasamy R, Ganesan N. Vibration and damping analysis of fluid filled orthotropic cylindrical shells with constrained viscoelastic damping. Comput Struct. 1999;70(3):363–376. doi: 10.1016/S0045-7949(98)00192-8

[88] Yang C, Jin G, Liu Z, et al. Vibration and damping analysis of thick sandwich cylindrical shells with a viscoelastic core under arbitrary boundary conditions. Int J Mech Sci. 2015;92:162–177. doi: 10.1016/j.ijmecsci.2014.12.003.

[89] Siddiqi KS, et al. Fabrication, characterization and cytotoxicity of spherical-shaped conjugated gold-cockle shell derived calcium carbonate nanoparticles for biomedical applications. Nanoscale Res Lett. 2018;13:1–17. doi: 10.1186/s11671-017-2411-3

[90] Siddiqi KS, et al. Recent status of nanomaterial fabrication and their potential applications in neurological disease management. Nanoscale Res Lett. 2018;13(1):231. doi: 10.1186/s11671-018-2638-7

[91] Singh R, Pantarotto D, McCarthy D, et al. Binding and condensation of plasmid DNA onto functionalized carbon nanotubes: toward the construction of nanotube-based gene delivery vectors. J Am Chem Soc. 2005;127(12):4388–4396. doi: 10.1021/ja0441561.